

Electric field reversals in dc negative glow discharges

Richard A. Gottscho, Annette Mitchell, Geoffrey R. Scheller, and Yin-Yee Chan
AT&T Bell Laboratories, Murray Hill, New Jersey 07974

David B. Graves
Department of Chemical Engineering, University of California, Berkeley, California 94720
(Received 12 June 1989)

Electric field reversals play an important role in maintaining glow discharges by determining the partitioning of ion flux between cathode and anode. For years, the existence of field reversals in the negative glow has been the subject of controversy. For a range of pressures, gas compositions, and electrode spacings, we observe field reversals using laser optogalvanic (LOG) spectroscopy: The discharge current is increased by excitation of molecular ions to a state with larger mobility. The sign of the LOG signal is a direct measure of the sign of the electric field. A single-beam electron model, where it is assumed that the glow is sustained by a monoenergetic, unidirectional beam of electrons emanating from the cathode, is in good agreement with most experimental observations. The model accurately predicts the existence of field reversals and the spatial dependence of both LOG and laser-induced fluorescence signals. By including momentum and energy dispersion in the beam, the model could be further improved.

I. INTRODUCTION

The presence of electric field reversals in the negative-glow region of dc discharges has been the subject of debate and controversy. For example, two popular texts show contradictory pictures of the negative glow—with and without field reversals.^{1,2} In the classic work of Druvestyn and Penning,³ the existence of an electric field reversal in the negative glow of a dc discharge was “guessed” to exist. More recently, Lawler *et al.* have assumed the existence of an electric field reversal in evaluating the current balance at the surface of a cold cathode discharge.⁴ They estimate the position of the field reversal by linearly extrapolating their spectroscopic field measurements from the sheath into the glow.

Electric field reversals play an important role in the self-maintenance of glow discharges and provide an important clue in distinguishing between different discharge models. One usually assumes that a field reversal exists in the negative glow and that the plasma potential floats above the anode potential. Thus, positive ions bombard both cathode and anode surfaces. One makes this assumption recognizing the disparity between electron and ion characteristic energies in a glow discharge and the resultant preferential loss of electrons by diffusion.³ The field reverses in the negative glow both to reduce electron loss and to enhance ion loss such that the total current is conserved from cathode to anode. The position in the negative glow where the field reverses marks the beginning of the presheath⁵ and determines the fraction of ions in the negative glow that are accelerated toward the cathode.⁴ This fraction, in turn, influences discharge maintenance mechanisms.

Consider two simple mechanisms for self-maintenance of a negative-glow dc discharge. If ionization took place predominantly in the cathode sheath, rapid electron loss

by diffusion and acceleration to the anode would be easily compensated by ion loss to the cathode and no field reversal would be necessary. Such a mechanism would be valid if electrons were in hydrodynamic equilibrium with the local electric field (local-field theory) or if ion and fast neutral impact ionization were the dominant source of ionization.^{6–8} On the other hand, if ionization occurred predominantly in the bulk plasma where fields are weak and ions are not easily extracted, field reversals would occur to constrain electron loss and enhance ion loss. Such a mechanism would be valid if the discharge were maintained by a flux of high-energy electrons emanating from the cathode and cathode fall region.^{6–9}

Under other circumstances, field reversals may not occur. For example, if a sufficiently large number of negative ions were present, the plasma potential need not float above the anode potential.¹⁰ Positive ions would be accelerated toward the cathode while electrons and negative ions would be accelerated toward the anode.

Recently, Walkup *et al.*¹¹ (hereafter referred to as WDA) reported laser optogalvanic (LOG) detection of molecular ions in dc glow discharges through N₂ and CO. They suggested that a change in ion mobility on excitation is responsible for the LOG effect. For an excited state with larger (smaller) mobility, a current increase (decrease) occurs on excitation. WDA also showed that the ionic LOG effect is weak or nonexistent for lower pressure discharges and for dilute mixtures in He. In both cases, the mobility description can be invalid.¹²

Several factors need to be considered when interpreting LOG signals resulting from ionic excitation. First, changes in recombination and diffusion could account for the signal. These mechanisms are not considered important compared to changes in ionic mobility because the excited state lives for too short a period compared to characteristic times for recombination and diffusion. On

the other hand, the excited-state lifetime is comparable to the mean time between charge exchange and velocity changing collisions. Second, the mobility approximation is not valid when the mean free path is long compared to the scale over which the electric field changes. Thus, the simple interpretation based on ion mobility changes may not be valid in the sheath but should be accurate in the glow where the field is weakly varying. In particular, the mobility description should be valid near field reversals. Thus, for small perturbations in current, the *sign* of the LOG signal should depend only on the sign of the electric field, and the LOG signal resulting from excitation of short-lived ionic states provides a direct measure of electric field reversals.

In this work, we use the LOG effect to measure electric field reversals in dc negative-glow discharges over a range of gas compositions, pressures, and electrode gaps. Under most circumstances, our results differ qualitatively and quantitatively from those of WDA. In particular, we observe electric field reversals and electric field double layers (extrema). WDA present no evidence and make no mention of electric field reversals or electric field double layers. Most of these differences can be attributed to differences in operating conditions (pressure, gap, gas composition) but even for nominally the same operating conditions, we find discrepancies between our results and theirs that can only be attributed to differences in reactor geometry. We presume that radial current loss in WDA's reactor provides the necessary ion loss to compensate for electron loss without establishing an electric field reversal. This is analogous to the field profile in a positive column.³

The N_2^+ molecular ion produced in discharges through N_2 and mixtures of N_2 and Ar is excited from its lowest and first excited vibrational levels while the change in discharge current is recorded. Along with density profiles of N_2^+ ($v=0$ and 1) probed using laser-induced fluorescence (LIF), the LOG signal is obtained as a function of position between plane parallel electrodes.

In the sections that follow, we first discuss the experimental approach (Sec. II) and results obtained (Sec. III). The data are compared to the output of a single-beam model in Sec. IV and our conclusions are summarized in Sec. V.

II. EXPERIMENTAL DETAILS

A. Reactor geometry, plasma confinement, and gas flow

Although details of the reactor design have been discussed previously,¹³ it is important to consider several aspects that differ from the reactor design used by WDA. Stainless-steel electrodes of 7.62-cm diameter are used and separated by distances ranging from 1 to 3 cm. The electrodes are contained within an 8-cm diameter 6-way Pyrex cross. Alumina cylinders are used to fill the space behind the electrode surfaces and prevent the current from flowing behind the electrodes. A current-regulated dc voltage is applied across the two electrodes in series with a 10-k Ω ballast resistor. The voltage tends to drift ($\lesssim 10\%$) slowly in time due to electrode heating and con-

tamination but both LOG and LIF signals are not significantly affected.

WDA used a stainless-steel cross of 4-cm diameter with 2.5-cm diameter electrodes separated by 1.2 cm. Under these conditions, it is likely that the plasma is not well confined between the two electrodes and the current flows to the reactor walls. The current may also flow behind the electrodes. These differences are most likely responsible for the differences observed in LOG signals as a function of position.

N_2 (99.999%) and Ar (99.999%) are supplied by Matheson and used without further purification. Gas flow and pressure are controlled using mass flow controllers and a downstream butterfly valve, respectively. Gas compositions quoted are determined from relative flow rates and represent mole fractions in the feedstock.

B. LOG and LIF measurements

Both the lowest ($v''=0$) and first excited ($v''=1$) vibrational levels of the $N_2^+ X^2\Sigma_g^+$ ground state are probed by exciting the $B^2\Sigma_u^+ - X^2\Sigma_g^+$ (0,0) and (0,1) bands, respectively. A pulsed nitrogen-pumped dye laser is used primarily to excite the (0,0) band. This is similar to the experiment of WDA. For excitation of the (0,1) hot band, an Ar⁺-pumped, cw dye laser is used.

1. Pulsed versus cw excitation

With the cw dye laser, a substantially better signal-to-noise ratio, S/N, is obtained in both LOG and LIF experiments because of the larger duty cycle (~ 0.5) for the cw laser relative to the pulsed laser ($\sim 10^{-6}$). For both laser excitation schemes, the transitions are easily saturated. However, in the LIF experiment, the S/N enhancement with the cw laser is only ~ 100 and not $\sim 10^6$ as expected from the ratio of duty cycles. For both types of excitation, the noise level is determined by the plasma glow. Since the cw laser linewidth (~ 1 MHz) is smaller than the Doppler width, only a small component of the velocity distribution is selected on excitation. The homogeneous linewidth (~ 0.03 GHz), resulting from pressure, power, and lifetime broadening, determines the fraction of molecules excited. With the pulsed laser, on the other hand, the laser linewidth (~ 20 GHz) is larger than both the Doppler linewidth (~ 2 GHz) and the spin splitting (~ 6 GHz) so ~ 200 times as many molecules are excited.¹⁴ Optical pumping of the ground state in the cw experiment also limits S/N.

For the LOG signal, the enhancement in S/N using the cw laser is larger (~ 1000 times). This is because the major source of noise in the LOG experiments with the pulsed laser is electromagnetic interference from the nitrogen laser. For cw laser excitation, the noise level is determined by fluctuations in discharge current. Because of the S/N enhancement, most of the results presented here were obtained using cw laser excitation.

2. Charge exchange

For pure N_2 discharges the population in $v''=1$ is so small that we could not detect it even with the cw dye

laser. This situation is remedied by adding Ar to the discharge, and taking advantage of the rapid charge exchange reaction,¹⁵



that populates both $v''=0$ and 1.

3. Detection schemes

LIF is collected and focused onto the slit of a monochromator as discussed previously.¹³ Spatial profiles are obtained by scanning both the laser beam steering optics and the fluorescence collecting optics synchronously. Typical spatial resolution is $\sim 200 \mu\text{m}$ axially (along an axis perpendicular to the electrode surfaces) and $\sim 1 \text{ cm}$ radially (parallel to the electrodes). For pulsed experiments, the transient photocurrent from an RCA C31034A or an EMI 9659QA photomultiplier tube is captured and integrated using a Stanford Research Instruments gated integrator with a 200-ns gate. For cw

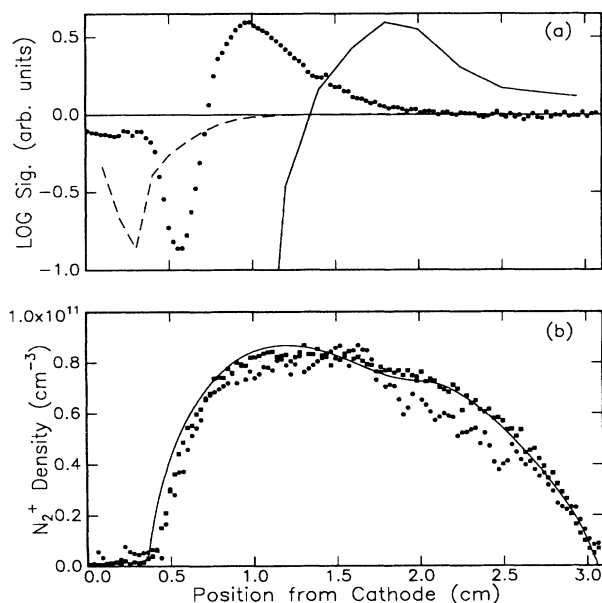


FIG. 1. (a) LOG and (b) LIF spatial profiles resulting from excitation of $P(12)$ in the $\text{N}_2^+ B^2\Sigma_u^+ - X^2\Sigma_g^+$ band system as a function of position from the cathode. The laser beam is unfocused and has a beam waist [FWHM (full width at half maximum)] of approximately 0.1 cm. The spatial resolution for LIF is $\lesssim 200 \mu\text{m}$ and is dictated by the spectrometer slit width. Note that the LOG signal crosses zero (field reversal) near but toward the cathode site of the N_2^+ density maximum. The \blacksquare 's and \bullet 's in (b) correspond to $v''=0$ and 1, respectively. The profiles are insensitive to the vibrational level probed. Results from a single-beam model are plotted as lines. For the LOG signal, the model results are plotted twice: once normalized to the positive maximum (solid line) and once normalized to the negative minimum (dashed line). For the LIF signal, the experimental data are normalized to the model calculations. Plasma conditions: 3.05-cm gap, 7.62-cm diameter, stainless-steel electrodes, 0.3 Torr, 9 sccm Ar, 1 sccm N_2 , 0.075 W cm^{-3} , 550 V, 0.42 mA cm^{-2} . Secondary emission coefficient used in simulation: 0.103.

experiments, the laser is modulated at 200 to 500 Hz with a 50% duty cycle and the LIF photocurrent is fed into a PAR 124A lockin amplifier.

For LOG detection, a high pass RC circuit is used for both pulsed and cw laser excitation. For pulsed excitation, the transient current is sampled using a Stanford Research Instruments gated integrator with a 200-ns gate. For cw excitation, the LOG current is sampled using a PAR HR-8 lockin amplifier. LOG spatial resolution is dictated by the laser excitation volume which is characterized by scanning the LIF profile using just fluorescence collection optics. For most results presented, the beam diameter (axial resolution) is $\sim 0.1 \text{ cm}$ and radially uniform. The LOG signal is an average over the radial dimension. For some profiles, the laser is loosely focused to obtain uniform axial resolution of $\sim 500 \mu\text{m}$ over the electrode diameter. However, the profiles are qualitatively similar for this higher spatial resolution, indicating that the characteristic scales over which LOG signals change are comparable to or larger than 0.1 cm. Note that since the laser is not expanded to match the diameter of the electrode, the experimental configuration is not cylindrically symmetric. This is consistent with the experiment of WDA.

III. LOG AND LIF PROFILES

Typical LOG and LIF spatial profiles for a range of pressures, compositions, and electrode spacings are shown in Figs. 1–3. In Fig. 1, both $v''=0$ and 1 data are shown to illustrate that profiles are insensitive to the vibrational level probed. Similarly, we find no dependence

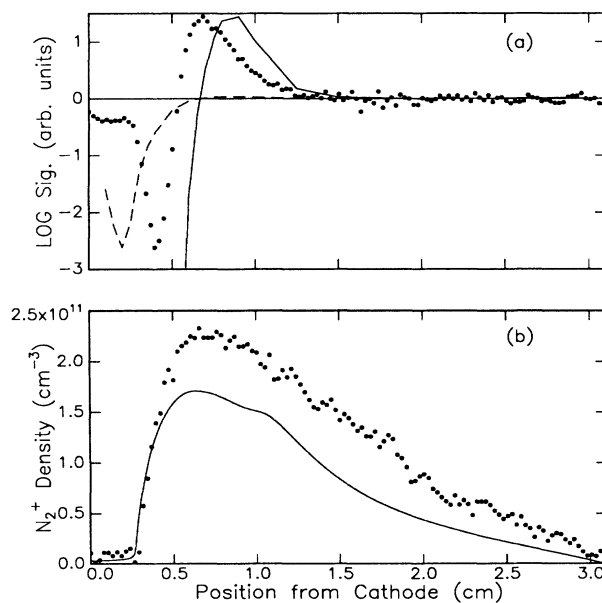


FIG. 2. Same as Fig. 1 except plasma conditions: 8 sccm Ar, 2 sccm N_2 , 0.14 W cm^{-3} , stainless-steel electrodes, gap=3.05 cm, diameter=7.62 cm, 560 V, 0.76 mA cm^{-2} , 0.5 Torr. LOG simulations are normalized to data as in Fig. 1. The same normalization to theory used in Fig. 1 is used here for LIF data. Secondary emission coefficient: 0.073.

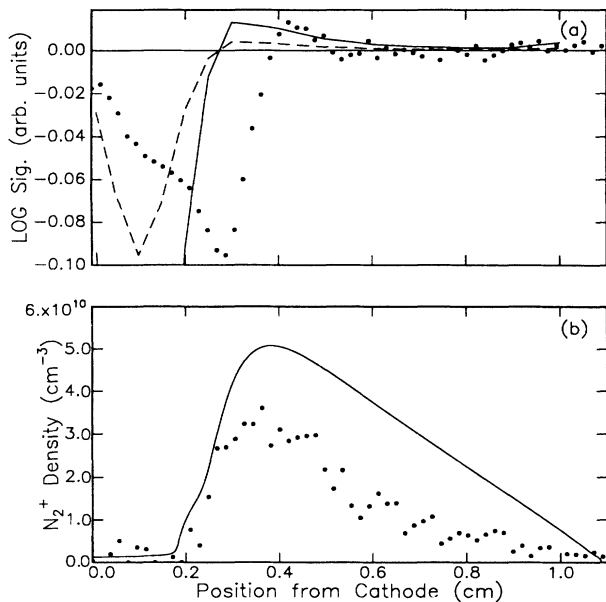


FIG. 3. Same as Fig. 1 except for plasma conditions: 9 sccm Ar, 1 sccm N₂, 0.25 W cm⁻³, 1.08-cm gap, 350 V, 0.77 mA cm⁻², 1.0 Torr. Note change in gap. These conditions are similar to and the profiles resemble those published by WDA. LOG simulations are normalized to data as in Fig. 1. The same normalization to theory used in Fig. 1 is used here for LIF data. Secondary emission coefficient: 0.044.

on the rotational level probed for $J \lesssim 20$. Hereafter, we show and discuss primarily $v''=1$ results obtained using the cw laser but the conclusions drawn apply to the N₂⁺ molecule regardless of vibrational and rotational level.

A. Electric field reversal

Several features in Figs. 1–3 should be noted. At low pressure, the LOG signal changes sign near the position of the N₂⁺ ion density maximum but slightly to the cathode side. *Note that the position of the N₂⁺ density maximum may not correspond to the total charge density maximum.* To the left of the electric field reversal, ions are extracted from the glow toward the cathode. These ions help maintain the glow by inducing secondary electron emission at the cathode. To the right of the field reversal, ions are accelerated toward the anode. These ions do little to help maintain the glow. At higher pressure, the field reversal occurs toward the anode side of the N₂⁺ density maximum. Under all conditions—higher pressure, smaller gaps, different gas compositions—we observe field reversals (Figs. 1–3).

B. Presheath and sheath

On the cathode side of the field reversal, the LOG signal first grows strongly negative (ion current increases toward the cathode) and then decreases near the cathode. The decrease in signal near the cathode is more pronounced at lower pressure where the mobility approximation is less valid. The large negative LOG signal coin-

cides with a falloff in ion density as measured by LIF. This region, called the presheath, feeds ions from the negative glow into the cathode fall. The electric field in the presheath as simulated in Sec. IV is smaller than 1 V/cm over the range of conditions investigated. Where the ion density is no longer detectable using LIF, the LOG signal diminishes rapidly. This marks the beginning of the cathode fall; the electric field gradient becomes large and ions are swept into the cathode. For the range of conditions investigated, the mobility limit is probably not valid in this region.

Close to the cathode, the falloff in LOG signal results from transit time effects.¹⁶ Ions excited in this region may impact the electrode before colliding with neutral gas molecules and atoms; and, in the absence of gas-phase collisions, ionic excitation does not produce an optogalvanic effect. Elsewhere in the cathode fall, the reduced LOG signal may result from smaller differences between excited- and ground-state collision cross sections for ions with higher translational energy acquired by acceleration in the sheath.

C. Charge double layers

Toward the anode side of the field reversal, the LOG signal increases, reaches a maximum, and then declines rapidly toward the anode. In this region, the electric field is weak and roughly constant (see Sec. IV); it is unlikely that collision cross sections vary spatially. The LOG signal decreases rapidly toward the anode because ions carry little current in this region (see Sec. IV). Because the field is weak, the ion drift velocity is small and most of the current is carried by electron diffusion. Thus, changing ion mobility by excitation does little to change the total discharge current.

The maximum in the LOG profile suggests that the electric field also exhibits a maximum. This is verified in Sec. V below using a single-beam model for the discharge. Such a double layer could result from the flux of hot electrons from the cathode fall into the negative glow. To conserve current, the bulk electron diffusion against the field must be slower where the beam current is significant. As the beam loses energy and merges into the bulk group, the field can decrease and allow larger bulk current.

Double layers usually occur when plasmas of different characteristic energy come into contact.¹⁷ For example, in a constricted dc positive column, the hot plasma in the narrow bore is isolated from the cold plasma in the wide bore by a double layer that acts to convert hot plasma into cold plasma and vice versa.¹⁸ In negative-ion-containing plasmas, a double layer appears to convert negative ions (“cold electrons”) into (“hot”) electrons.^{7,10} In semiconducting *pn* junctions, ionized acceptors and donors act as cold plasma while electrons and holes act as hot plasma.¹⁹ For the cathode fall—negative-glow transition here, beam electrons created at the cathode and amplified in the cathode fall are hot. Bulk electrons trapped in the glow and thermalized by collisions with background neutral gas are cold.

IV. SINGLE-BEAM MODEL SIMULATIONS

As stated in Sec. I, one reason for measuring field reversals is to test discharge models. It has been shown

previously that the local-field model fails to predict field reversals.^{6,8} In this section we briefly describe a single-beam model we used to simulate profiles in Figs. 1–3. A major limitation in these simulations is lack of precise collision cross sections for excited-state ionic transport in N₂-Ar gas mixtures.

The LOG signal is assumed to arise everywhere and under all conditions from a change in mobility upon excitation. As mentioned above, this assumption is probably not correct for the sheath and, indeed, the agreement between experiment and model is poor in this region (see below). The change in mobility is assumed to be independent of the electric field strength; again, this is reasonable only in the weak-field glow which is where field reversals occur. Thus, the LOG signal is assumed to be proportional to the local electric field and local ion density. Because of the dearth in excited-state cross-section data, we make the simplifying assumption that the change in mobility is simply 10⁻⁴ times the ground-state mobility, i.e., the excited state is slightly more mobile. The spatial dependence of the calculated LOG signal does depend significantly on the magnitude of this mobility change. The value chosen is commensurate with experimental magnitudes for the LOG signal, but must be viewed as a phenomenological parameter because of the assumptions mentioned above and the inherent transverse averaging in the experiment that is not accounted for by the one-dimensional model. It is beyond the scope of this work to model the 2D aspects of the LOG experiment. Moreover, considering the lack of cross-section data available, the effort seems unwarranted at this time. Thus, we look for qualitative insights when modeling LOG data.

A. Assumptions and parameters

The basic assumption behind the single-beam model is that electrons created at the cathode form a monoenergetic, unidirectional beam as they traverse the cathode fall.^{8,9} In the sheath, ionizing collisions by beam electrons produce additional beam electrons and the beam exhibits gain. In the glow, ionizing collisions produce bulk electrons and the beam loses energy. When the beam energy falls below the ionization threshold, beam electrons are rapidly converted into bulk electrons. Equations for beam flux and energy are solved simultaneously with Poisson's equation and equations for ion continuity and bulk electron continuity. Although crude, the single-beam model works well in describing discharges where E/N , the electric field to density ratio,

is large but uniform. Previously,⁶ we suggested that discrepancies between single-beam model predictions and experiment occur because the beam propagates too far into the glow. Neglect of momentum transfer and energy dispersion of the beam are the cause. Recent Monte Carlo simulations confirm this interpretation.²⁰ This problem is "fixed" *ad hoc* as described below.

An asset of the single-beam model is its use of energy-dependent electron-impact collision cross sections. Provided these are known, the number of free parameters is significantly constrained. The cross-section set used here is slightly modified and expanded from that used previously. Both the excitation and ionization cross sections for Ar and N₂ are expressed in a convenient analytical form

$$\sigma = \frac{\phi A}{\epsilon \epsilon_{\text{th}}} \left[\ln \left[\frac{\epsilon}{\epsilon_{\text{th}}} \right] + \sum_{i=1}^4 B_i (1 - \epsilon_{\text{th}}/\epsilon)^i \right], \quad (2)$$

where A , B_i , and the threshold energy ϵ_{th} are given in Table I. The beam energy is given by ϵ and is obtained by a self-consistent solution of the set of equations as mentioned above and described in greater detail elsewhere.^{6,8,9} The cross section set for Ar is the same as that used previously.⁶ For N₂, the sets compiled in Ref. 21 were used. For N₂ excitation, the cross section is truncated below 9.92 eV because beam electrons are converted into bulk electrons at a rapid rate below the ionization threshold of 15.58 eV.^{6,8,20} Thus, the details of vibrational and rotational excitation of N₂ are not considered.

To "fix" the problem of excessive penetration into the glow, the parameter $\phi=2$ is included. This value is determined by forcing agreement in the position of the N₂⁺ density maximum for the experimental data shown in Fig. 2. The same value multiplies both Ar and N₂ cross sections and is fixed for all other pressures, gas compositions, and electrode gaps.

Since secondary emission coefficients are unknown for ion, metastable, and photon impact generation of beam electrons at the cathode, it is necessary to adjust at least one of these in the model. In principle, these numbers could be obtained from experimental data, however, the cathode surface structure and composition in these experiments is neither well controlled nor well characterized. In addition, ion, metastable, and photon fluxes and energy distributions are unknown. Therefore, the ion secondary emission coefficient is adjusted (all other coefficients are set to zero) to obtain agreement with experimental

TABLE I. Excitation and ionization cross-section parameters.

Cross section	$\frac{A}{(\text{\AA}^2 \text{eV}^2)}$	B_1	B_2	B_3	B_4	ϵ_{th} (eV)	Ref.
Ar excitation	477	-0.789	1.900	-0.824	0.208	11.5	a
Ar ionization	2334	-0.581	0.098	-1.146	2.440	15.76	b
N ₂ excitation	1737	-0.568	-0.022	-1.127	0	9.92	c
N ₂ ionization	5249	-0.921	-0.633	0.181	0	15.58	c

^aE. Eggarter, J. Chem. Phys. **62**, 833 (1975).

^bW. Lotz, Z. Phys. **232**, 101 (1970).

^cA. V. Phelps and L. C. Pitchford, Phys. Rev. A **31**, 2932 (1985).

TABLE II. Single-beam model parameters.

		Ref.
Bulk electron diffusivity	$ND_e = 2.5 \times 10^{21} \text{ cm}^{-1} \text{ s}^{-1}$	a
Bulk electron drift velocity	$NW_e = -1.06 \times 10^{22} \text{ E cm}^2 \text{ V}^{-1} \text{ s}^{-1}$	a
Bulk electron temperature	$T_e = 0.25 \text{ eV}$	
Ion diffusivity	$ND_p = 3.53 \times 10^{18} \text{ cm}^{-1} \text{ s}^{-1}$	
Ar ⁺ -N ₂ charge exchange cross section ^b	$\sigma_{ce} = 2.2 \times 10^{-11} \text{ cm}^3 \text{ s}^{-1}$	b
N ₂ ⁺ recombination cross section	$\sigma_r = 1.4 \times 10^{-6} (0.0258/T_e)^{0.41} \text{ cm}^3 \text{ s}^{-1}$	c
Beam-to-bulk transfer cross section	$\sigma_{bb} = 2.175 \times 10^{-16} \text{ cm}^2$	d

^aA. L. Ward, *J. Appl. Phys.* **33**, 2789 (1962).

^bJ. B. Laudenslager, W. T. Huntress, and M. T. Bowers, *J. Chem. Phys.* **61**, 4600 (1974).

^cJ. Wm. McGowan and J. B. A. Mitchell, in *Electron-Molecule Interactions and their Applications*, edited by L. G. Christophorou (Academic, Orlando, 1984), Vol. 2, p. 65.

^dR. A. Gottscho, A. Mitchell, G. R. Scheller, N. L. Schryer, D. B. Graves, and J. P. Bouef, *Proceedings of Seventh Symposium on Plasma Processing, Electrochemical Society*, edited by G. S. Mathad, G. C. Schwartz, and D. W. Hess [Electrochem. Soc. **88-22**, 1 (1988)].

current densities. The values used are given in the captions to Figs. 1–3.

The bulk electron temperature T_e is also a critical parameter. For N₂⁺, dissociative ion-electron recombination is an important loss mechanism that is sensitive to T_e .²² The charge double layer mentioned above and the magnitude of the electric field are also dependent on the value of T_e (see below). T_e is adjusted to obtain good agreement for the LIF data shown in Fig. 2 and then fixed for all other pressures, compositions, and electrode gaps. The value obtained, 0.25 eV, is given along with other model parameters in Table II. In fact, it would be reasonable to adjust T_e for changes in these plasma parameters but we found this unnecessary.

A few comments concerning ionic drift velocities are also warranted. Since we were unable to find values for N₂⁺ drift velocities in Ar over the range of fields necessary, we set them equal to those in pure N₂ as given by Ward.²³ Similarly, the Ar⁺ drift velocity is obtained from Ward's paper as before and not adjusted for 10–20% N₂ dilution. Ward's velocity parameters are fit to a more convenient analytical form,

$$W = \frac{W_1 E}{1 + W_2 E^{1/2}}, \quad (3)$$

where W_1 and W_2 are given in Table III for the three pressures considered. To determine the consequences of these assumptions, we changed W_1 by 2 times and found

TABLE III. Ion mobility parameters.

Pressure (Torr)	W_1 (m ² /V s)	W_2 (m/V) ^{1/2}
	Ar ⁺	
1.0	0.574	0.066
0.5	1.819	0.152
0.3	4.294	0.281
	N ₂ ⁺	
1.0	731.2	90.1
0.5	1025	90.1
0.3	1319	90.1

little difference in the spatial profiles. The primary effect is in the total discharge current density and absolute ion density which is compensated for by adjusting the secondary emission coefficient.

Both N₂⁺ and Ar⁺ are formed by electron-impact ionization from the respective neutrals. In addition, N₂⁺ can be formed by charge transfer as described in Eq. (1). The rate constant for this reaction is taken from Ref. 15 and is given in Table II for a neutral gas temperature of 350 K. Clustering of N₂⁺ to form N₃⁺ and N₄⁺ is unimportant for dilute mixtures of N₂ in Ar over the range of pressures considered here.^{24,25}

B. Model results

1. Successes

On comparing experimental and model results in Figs. 1–3, one is struck by the qualitative accuracy of the model. The model accurately predicts (1) occurrence of field reversals near the ion density maximum, (2) the maximum in the LOG signal on the anode side of the field reversal, (3) the falloff in LOG signal toward the anode, and (4) the shapes and magnitudes of the N₂⁺ ion density as measured by LIF.

The existence of field reversals is necessary to constrain electron loss and enhance ion loss as discussed in Sec. I. Because the beam model includes ionization in the weak-field negative-glow region, the field reverses. By contrast, the local-field model fails to predict the existence of field reversals because too much ionization occurs in the sheath.^{6,8}

The maximum in the LOG signal on the anode side of the field reversal results from a maximum in the electric field (Fig. 4). As discussed above, a double layer forms because of the injection of hot electrons from the cathode fall into the cold glow. This interpretation is supported by simulations where the bulk electron temperature T_e is increased above 0.50 eV and the double layer disappears. Instead, a more uniform field of comparable magnitude (~5 V/cm) persists throughout the glow to reduce the electron loss.

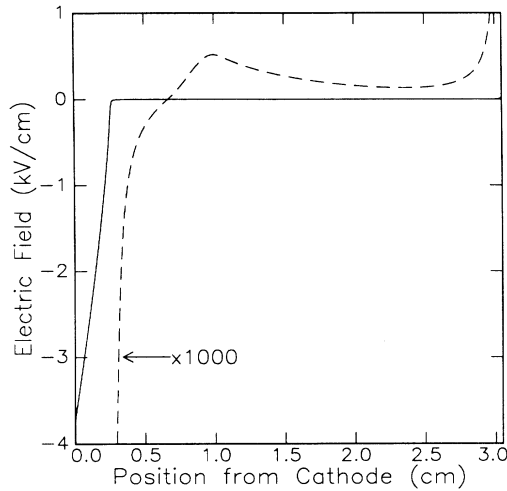


FIG. 4. Beam model electric field corresponding to conditions given in Fig. 2. To show the double layer and weak field in the negative glow, the field is multiplied by 1000 times and plotted as a dashed line.

The good agreement between model and experimental LOG signal shapes as a function of position on the anode side of the field reversal results from the weak field in this region. The assumption of constant change in ion mobility is reasonable under these conditions. The falloff in the LOG signal can be understood by examining model results for charged particle fluxes in Fig. 5. Toward the anode, electron (diffusion) current dominates as the field decreases. Because the field is small, the ion current is negligible. Thus, when the ion mobility is changed by laser excitation, little change occurs in the total discharge current.

The small value for the electric field in the glow is a consequence of the small value for T_e . The field in the glow is established to constrain electron loss and enhance ion loss. Thus, for cold electrons, only a small field is needed.

The good agreement between the single-beam model and experimental LIF profiles is somewhat spurious since the parameter ϕ is included and the densities are normalized to theory for one set of conditions. Nonetheless, the agreement obtained for different pressures, compositions, and gaps without further adjustment of these parameters is encouraging. It suggests that proper accounting of momentum transfer and energy dispersion in the beam should improve the model significantly.²⁰ Measurement of the absolute ion density would provide a more stringent test of the theory by eliminating the need for normalization. It would also provide an additional constraint on T_e . The small discrepancies in density magnitudes that are apparent in Figs. 1–3 most likely result from the use of ϕ and neglect of vibrational relaxation that could be an important loss mechanism for $v''=1$ at higher pressure.

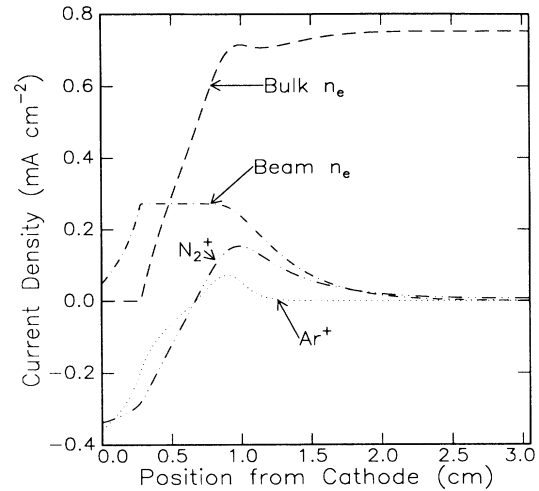


FIG. 5. Beam model current densities as a function of position for the conditions given in Fig. 2. Note the dominance of electron (diffusion) current in the negative glow.

2. Failings

One is also struck by failings of the model: (1) the relative magnitudes of negative and positive LOG signals are in poor agreement with experiment particularly at lower pressure, and (2) the position of the field reversal is not in accord with experiment. The discrepancy in the cathode fall and the disparity in scaling between cathode fall and negative-glow signals is indicative that the assumption of constant mobility change is not valid. This is not surprising since the field in the cathode fall is large and changing rapidly.^{26,27}

The failure of the model to predict the precise location of the field reversal probably results from the *ad hoc* parameter ϕ and the neglect of gradients in T_e . One expects T_e to be larger near the cathode than near the anode.

V. CONCLUSIONS

We have observed directly the presence of electric field reversals in dc negative-glow discharges that determine the partitioning of ion fluxes to anode and cathode. The ion flux to the cathode maintains the glow by inducing secondary electron emission. The field reverses in the negative glow in order to maintain current continuity: Ion loss to the anode is enhanced by the field while electron loss is constrained.

A single-beam model that assumes the discharge is maintained by a flux of monoenergetic, unidirectional electrons from the cathode is in good agreement with most experimental observations over a range of pressures, gas compositions, and electrode spacings. In particular, the model accurately predicts (1) existence of field reversals, (2) a charge double layer near the field reversal resulting from injection of hot electrons into the cold bulk, and (3) ion density magnitudes and spatial distributions.

The model fails to accurately predict the position of

the field reversal and the relative magnitudes of LOG signals in the cathode fall and negative glow. Of these, the second most likely results from the simplistic assumption concerning change in ion mobility on excitation that is necessitated by lack of precise cross-section data. The inaccuracy in the prediction for the position of the field reversal results from the monoenergetic and unidirectional assumptions about the beam electrons. The model should be improved substantially by accounting for momentum balance and energy dispersion of the beam electrons.

ACKNOWLEDGMENTS

We are grateful to Norm Schryer and Jean-Pierre Boeuf for their assistance in setting up the single-beam model program. We are also grateful to Jim Lawler and Will Allis for stimulating discussions on the nature of the negative glow to cathode fall transition, the significance of electric field reversals, and a critical reading of this manuscript. Bob Walkup generously shared with us details of his experimental arrangement.

-
- ¹B. Chapman, *Glow Discharge Processes* (Wiley, New York, 1980).
- ²A. von Engel, *Ionized Gases* (Clarendon, Oxford, 1965).
- ³M. J. Druyvesteyn and F. M. Penning, *Rev. Mod. Phys.* **12**, 87 (1940).
- ⁴D. A. Doughty, E. A. Den Hartog, and J. E. Lawler, *Phys. Rev. Lett.* **58**, 2668 (1987); E. A. Den Hartog, D. A. Doughty, and J. E. Lawler, *Phys. Rev. A* **38**, 2471 (1988).
- ⁵F. F. Chen, *Introduction to Plasma Physics* (Plenum, New York, 1985).
- ⁶R. A. Gottscho, A. Mitchell, G. R. Scheller, N. L. Schryer, D. B. Graves, and J. P. Boeuf, *Proceedings of the Seventh Symposium on Plasma Processing, Electrochemical Society*, edited by G. S. Mathad, G. C. Schwartz, and D. W. Hess [Electrochem. Soc. **88-22**, 1 (1988)].
- ⁷J. P. Boeuf, *Phys. Rev. A* **36**, 2782 (1987).
- ⁸J. P. Boeuf and P. Segur, in *Interactions Plasma Froids Matériaux*, edited by C. Lejeune (Les Editions de Physique, Les Ulis Cedex, France, 1988), p. 113.
- ⁹A. V. Phelps, B. M. Jelenkovic, and L. C. Pitchford, *Phys. Rev. A* **36**, 5327 (1987); B. M. Jelenkovic and A. V. Phelps, *ibid.* **36**, 5310 (1987).
- ¹⁰R. A. Gottscho and C. E. Gaebe, *IEEE Trans. Plasma Sci.* **14**, 92 (1986); *J. Vac. Sci. Technol. A* **4**, 1795 (1986).
- ¹¹R. Walkup, R. W. Dreyfus, and Ph. Avouris, *Phys. Rev. Lett.* **50**, 1846 (1983).
- ¹²J. E. Lawler, *Phys. Rev. A* **32**, 2977 (1985).
- ¹³R. A. Gottscho, G. Smolinsky, and R. H. Burton, *J. Appl. Phys.* **53**, 5908 (1982); R. A. Gottscho, G. P. Davis, and R. H. Burton, *Plasma Chem. Plasma Proc.* **3**, 193 (1983); *J. Vac. Sci. Technol. A* **1**, 622 (1983); R. A. Gottscho, R. H. Burton, D. L. Flamm, V. M. Donnelly, and G. P. Davis, *J. Appl. Phys.* **55**, 2707 (1984).
- ¹⁴K. A. Dick, W. Benesch, H. M. Crosswhite, S. G. Tilford, R. A. Gottscho, and R. W. Field, *J. Mol. Spectrosc.* **69**, 95 (1978).
- ¹⁵J. B. Laudenslager, W. T. Huntress, and M. T. Bowers, *J. Chem. Phys.* **61**, 4600 (1974).
- ¹⁶A. Margulis and J. Jolly, *Rev. Phys. App.* **24**, 323 (1989).
- ¹⁷N. Hershkowitz, *Space Sci. Rev.* **41**, 351 (1985); J. S. Levine and F. W. Crawford, *J. Plasma Phys.* **23**, 223 (1979).
- ¹⁸R. N. Franklin, *Plasma Phenomena in Gas Discharges* (Clarendon, Oxford, 1976).
- ¹⁹S. M. Sze, *Semiconductor Devices* (Wiley, New York, 1985).
- ²⁰M. Surendra, D. B. Graves, and G. M. Jellum, *Phys. Rev. A* (to be published).
- ²¹Y. Itikawa, M. Hayashi, A. Ichimura, K. Onda, M. Nakamura, H. Nishimura, and T. Takayanagi, *J. Phys. Chem. Ref. Data* **15**, 985 (1986); A. V. Phelps and L. C. Pitchford, *Phys. Rev. A* **31**, 2932 (1985).
- ²²J. Wm. McGowan and J. B. A. Mitchell, in *Electron-Molecule Interactions and their Applications*, edited by L. G. Christophorou (Academic, Orlando, 1984), Vol. 2, p. 65.
- ²³A. L. Ward, *J. Appl. Phys.* **33**, 2789 (1962).
- ²⁴P. F. Knewstubb and A. W. Tickner, *J. Chem. Phys.* **36**, 674 (1961); **37**, 2941 (1962).
- ²⁵D. Smith and N. G. Adams, *Pure Appl. Chem.* **56**, 175 (1984).
- ²⁶C. A. Moore, G. P. Davis, and R. A. Gottscho, *Phys. Rev. Lett.* **52**, 538 (1984); M. L. Mandich, C. E. Gaebe, and R. A. Gottscho, *J. Chem. Phys.* **83**, 3349 (1985); R. A. Gottscho, *Phys. Rev. A* **36**, 2233 (1987); J. Derouard, and N. Sadeghi, *Opt. Commun.* **57**, 239 (1986).
- ²⁷D. K. Doughty and J. E. Lawler, *Appl. Phys. Lett.* **45**, 611 (1984); B. N. Ganguly and A. Garscadden, *ibid.* **46**, 540 (1985).